

| | | | | | |
|---|-------------------|--------------------------------|--|---|--|
| REPORT DOCUMENTATION PAGE | | | Form Approved OMB NO. 0704-0188 | | |
| <p>The public reporting burden for this collection of information is estimated to average 1 hour per response, including the time for reviewing instructions, searching existing data sources, gathering and maintaining the data needed, and completing and reviewing the collection of information. Send comments regarding this burden estimate or any other aspect of this collection of information, including suggestions for reducing this burden, to Washington Headquarters Services, Directorate for Information Operations and Reports, 1215 Jefferson Davis Highway, Suite 1204, Arlington VA, 22202-4302. Respondents should be aware that notwithstanding any other provision of law, no person shall be subject to any penalty for failing to comply with a collection of information if it does not display a currently valid OMB control number.</p> <p>PLEASE DO NOT RETURN YOUR FORM TO THE ABOVE ADDRESS.</p> | | | | | |
| 1. REPORT DATE (DD-MM-YYYY) 05-01-2012 | | 2. REPORT TYPE Final Report | | 3. DATES COVERED (From - To) 9-Dec-2010 - 6-Jun-2011 | |
| 4. TITLE AND SUBTITLE Final Technical Report | | | 5a. CONTRACT NUMBER | | |
| | | | 5b. GRANT NUMBER W911NF-11-C-0044 | | |
| | | | 5c. PROGRAM ELEMENT NUMBER 665502 | | |
| 6. AUTHORS Yuliya B. Zotova | | | 5d. PROJECT NUMBER | | |
| | | | 5e. TASK NUMBER | | |
| | | | 5f. WORK UNIT NUMBER | | |
| 7. PERFORMING ORGANIZATION NAMES AND ADDRESSES ArkLight, Inc. PO Box 2 Center Valley, PA 18034 - | | | 8. PERFORMING ORGANIZATION REPORT NUMBER | | |
| 9. SPONSORING/MONITORING AGENCY NAME(S) AND ADDRESS(ES) U.S. Army Research Office P.O. Box 12211 Research Triangle Park, NC 27709-2211 | | | 10. SPONSOR/MONITOR'S ACRONYM(S) ARO | | |
| | | | 11. SPONSOR/MONITOR'S REPORT NUMBER(S) 59148-EL-SB1.1 | | |
| 12. DISTRIBUTION AVAILABILITY STATEMENT Approved for Public Release; Distribution Unlimited | | | | | |
| 13. SUPPLEMENTARY NOTES The views, opinions and/or findings contained in this report are those of the author(s) and should not be construed as an official Department of the Army position, policy or decision, unless so designated by other documentation. | | | | | |
| 14. ABSTRACT Report developed under topic #A10-076, contract W911NF-11-C-0044. The purpose of the work is to make a proof-of-concept demonstration on THz generation by using a dual-frequency laser in a nonlinear crystal. We have achieved all the objectives set for Phase I. In particular, we designed CW and Q-switched Yb:YAG lasers, purchased all the components necessary, assembled them into laser systems, optimized the setups, and tested the performances of the CW and Q-switched laser systems. Such laser systems were pumped by diode lasers at 940 nm. | | | | | |
| 15. SUBJECT TERMS SBIR Report | | | | | |
| 16. SECURITY CLASSIFICATION OF: | | | 17. LIMITATION OF ABSTRACT UU | 15. NUMBER OF PAGES | 19a. NAME OF RESPONSIBLE PERSON Yuliya Zotova |
| a. REPORT UU | b. ABSTRACT UU | c. THIS PAGE UU | | | 19b. TELEPHONE NUMBER 610-867-9794 |

Report Title

Final Technical Report

ABSTRACT

Report developed under topic #A10-076, contract W911NF-11-C-0044. The purpose of the work is to make a proof-of-concept demonstration on THz generation by using a dual-frequency laser in a nonlinear crystal. We have achieved all the objectives set for Phase I. In particular, we designed CW and Q-switched Yb:YAG lasers, purchased all the components necessary, assembled them into laser systems, optimized the setups, and tested the performances of the CW and Q-switched laser systems. Such laser systems were pumped by diode lasers at 940 nm. We achieved the broadband emission from the CW laser system. By placing an etalon in the laser cavities, we generated a pair of the output wavelengths around 1 micron from the CW and Q-switched laser systems. As a result, we successfully demonstrated the dual-frequency operation of the CW and Q-switched laser systems. Using the Q-switched dual-frequency laser, we generated THz pulses in a GaP crystal based on difference-frequency generation. We also confirmed the polarizations of the THz output pulses. Based on our calculations, the THz output powers can reach 8.5 mW through optimizations. We developed a concrete plan for identification and detection of biological agents, which is regarded as the major application of the THz spectrometer.

Enter List of papers submitted or published that acknowledge ARO support from the start of the project to the date of this printing. List the papers, including journal references, in the following categories:

(a) Papers published in peer-reviewed journals (N/A for none)

| <u>Received</u> | <u>Paper</u> |
|-----------------|--------------|
|-----------------|--------------|

TOTAL:

Number of Papers published in peer-reviewed journals:

(b) Papers published in non-peer-reviewed journals (N/A for none)

| <u>Received</u> | <u>Paper</u> |
|-----------------|--------------|
|-----------------|--------------|

TOTAL:

Number of Papers published in non peer-reviewed journals:

(c) Presentations

Number of Presentations: 0.00

Non Peer-Reviewed Conference Proceeding publications (other than abstracts):

| <u>Received</u> | <u>Paper</u> |
|-----------------|--------------|
|-----------------|--------------|

TOTAL:

Number of Non Peer-Reviewed Conference Proceeding publications (other than abstracts):

Peer-Reviewed Conference Proceeding publications (other than abstracts):

| <u>Received</u> | <u>Paper</u> |
|-----------------|--------------|
|-----------------|--------------|

TOTAL:

Number of Peer-Reviewed Conference Proceeding publications (other than abstracts):

(d) Manuscripts

Received

Paper

TOTAL:

Number of Manuscripts:

Books

Received

Paper

TOTAL:

Patents Submitted

Patents Awarded

Awards

Graduate Students

| NAME | PERCENT SUPPORTED | Discipline |
|-----------------|-------------------|------------|
| Pu Zhao | 0.50 | |
| FTE Equivalent: | 0.50 | |
| Total Number: | 1 | |

Names of Post Doctorates

| NAME | PERCENT SUPPORTED |
|-----------------|-------------------|
| Srinivasa Ragam | 0.50 |
| FTE Equivalent: | 0.50 |
| Total Number: | 1 |

Names of Faculty Supported

| NAME | PERCENT SUPPORTED |
|-----------------|-------------------|
| FTE Equivalent: | |
| Total Number: | |

Names of Under Graduate students supported

| | |
|------------------------|--------------------------|
| <u>NAME</u> | <u>PERCENT SUPPORTED</u> |
| FTE Equivalent: | |
| Total Number: | |

| | |
|--|------|
| Student Metrics | |
| This section only applies to graduating undergraduates supported by this agreement in this reporting period | |
| The number of undergraduates funded by this agreement who graduated during this period: | 0.00 |
| The number of undergraduates funded by this agreement who graduated during this period with a degree in science, mathematics, engineering, or technology fields:..... | 0.00 |
| The number of undergraduates funded by your agreement who graduated during this period and will continue to pursue a graduate or Ph.D. degree in science, mathematics, engineering, or technology fields:..... | 0.00 |
| Number of graduating undergraduates who achieved a 3.5 GPA to 4.0 (4.0 max scale):..... | 0.00 |
| Number of graduating undergraduates funded by a DoD funded Center of Excellence grant for Education, Research and Engineering:..... | 0.00 |
| The number of undergraduates funded by your agreement who graduated during this period and intend to work for the Department of Defense | 0.00 |
| The number of undergraduates funded by your agreement who graduated during this period and will receive scholarships or fellowships for further studies in science, mathematics, engineering or technology fields: | 0.00 |

Names of Personnel receiving masters degrees

| |
|----------------------|
| <u>NAME</u> |
| Total Number: |

Names of personnel receiving PHDs

| |
|----------------------|
| <u>NAME</u> |
| Total Number: |

Names of other research staff

| | |
|------------------------|--------------------------|
| <u>NAME</u> | <u>PERCENT SUPPORTED</u> |
| FTE Equivalent: | |
| Total Number: | |

Sub Contractors (DD882)

Inventions (DD882)

Scientific Progress

Technology Transfer

Final Technical Report

June 15, 2011

W911NF-11-C-0044

Period of Performance December 9, 2010 – June 6, 2011

“Widely-tunable, compact, and portable terahertz source based on intracavity difference-frequency generation in dual-frequency Yb:YAG laser for identification and detection of biological agents”

Purchase Request Number: 59148ELSB110230

Project: A10-076

CLIN 0001AF

Yuliya B. Zotova

ArkLight

P. O. Box 2

Center Valley, PA 18034

Results of the Phase I Work

Within the first month, we have made significant progress in order to meet the Phase-I objective #1 being set in our proposal, i.e. “To demonstrate dual-frequency operation of CW and Q-switched Yb:YAG lasers”. In particular, we designed a CW Yb:YAG laser. We then purchased all the components necessary and assembled them into a laser system. Fig. 1 illustrates a simplified setup for our first CW Yb:YAG laser. Such a laser system consists of a simple cavity made of an output coupler and a back reflector. The back reflector was realized after coating one end of the Yb:YAG crystal with its reflectivity reaching 99.8% at 1030 nm and its transmittance of 90% at 940 nm. The Yb:YAG crystal has the doping concentration of 5% and dimension of 5 mm (diameter) \times 5 mm (thickness). The distance between the two cavity mirrors was set to 3 cm for achieving the optimal performance. Such an Yb:YAG laser was pumped by a CW diode laser at the output wavelength of about 940 nm. We measured the spectrum of the pump laser diode, see Fig. 2. One can see that the output wavelength was measured to be 934.4 nm, which is close to the specified output wavelength of 940 nm. We then measured the output power as a function of the current being used to drive the laser diode. According to Fig. 3, the dependence measured by us is more or less linear, which is consistent with the characteristics for a solid-state laser [1]. By linearly fitting the data in Fig. 3, we deduced the threshold pump current for the laser diode to be 601 mA.

Using an output coupler with its reflectivity of 98%, we measured the output power from the CW Yb:YAG laser as a function of the driving current for the pump laser diode. Using Fig. 3, we then plotted the output power from the CW Yb:YAG laser as a function of the pump power from the diode

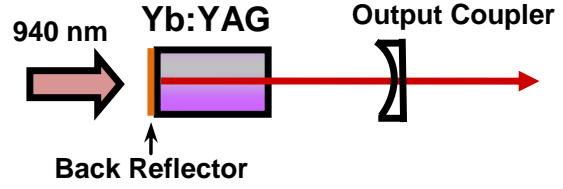


Fig. 1. A simplified experimental setup for a CW Yb:YAG laser designed by us.

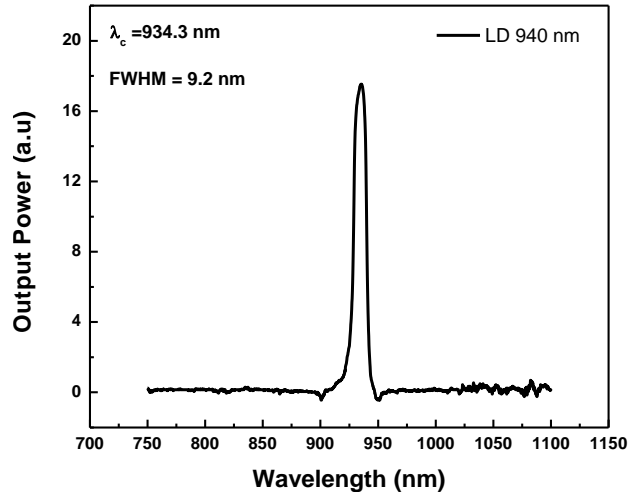


Fig. 2. A spectral profile of the output power from the pump laser diode, measured by using a spectrometer. The linewidth of 9.2 nm, measured here, is actually the spectral resolution of the spectrometer.

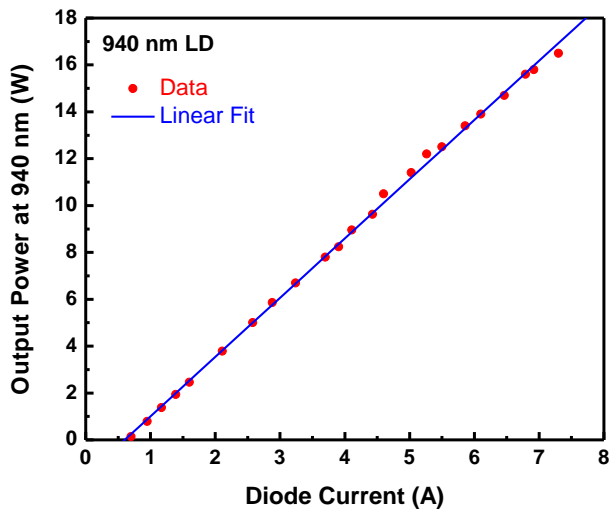


Fig. 3. Output power from the pump laser diode vs. driving current of the pump laser diode.

laser, see Fig. 4. One can see that the threshold pump power is determined to be 1.61 W by linearly fitting the data in Fig. 4. We also measured the spectral profiles of the Yb:YAG output powers at different pump powers of the laser diode, see Fig. 5. One can see that the center lasing wavelength was measured to be 1038 nm. Moreover, as the pump power for the laser diode was increased, the linewidth of the output power for the Yb:YAG laser was first increased linearly and then approached the severe saturation, see Fig. 6. Such a behavior is consistent with the characteristics of the Yb:YAG laser [1]. The linewidth of the laser output power reached 19.4 nm at the pump power of 9 W. Such a linewidth is indeed sufficiently wide for us to generate two wavelengths within the linewidth, which are necessary for THz generation in nonlinear crystals.

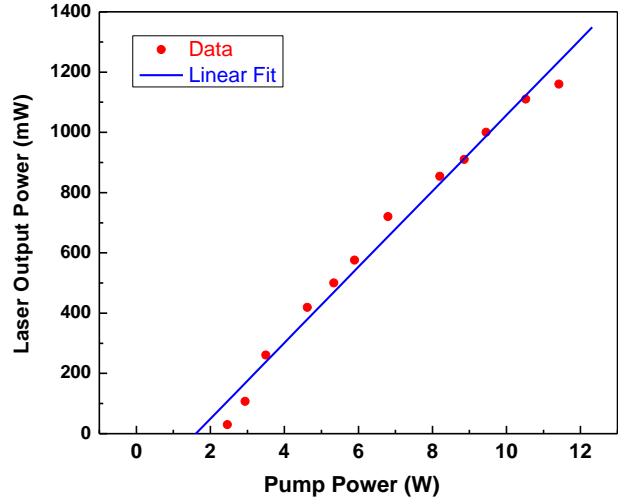


Fig. 4. Output power produced by a CW Yb:YAG laser vs. pump power from the pump laser diode at 940 nm.

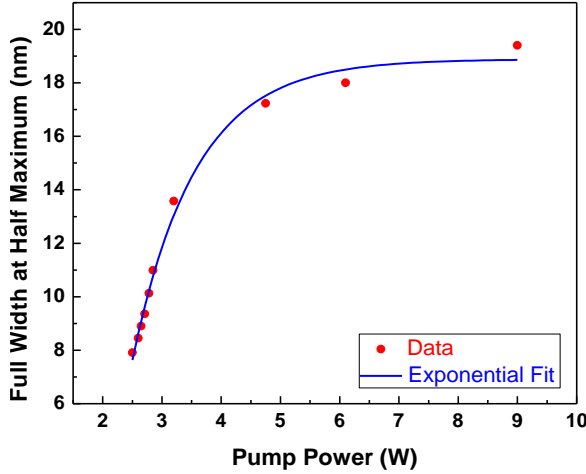


Fig. 5. Spectra of the output powers from the CW Yb:YAG laser at different powers of the pump laser diode.

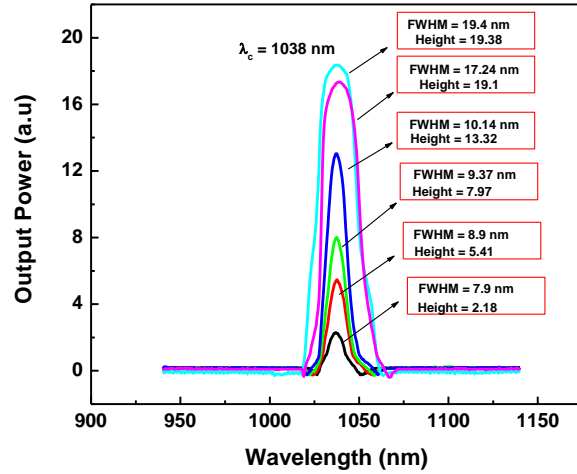


Fig. 6. Linewidth of the output power from the CW Yb:YAG laser is plotted vs. power of the pump laser diode.

Within the second month, we have made significant progress in order to meet the Phase-I objective #1 being set in our proposal, i.e. “To demonstrate dual-frequency operation of CW and Q-switched Yb:YAG lasers”. In particular, we optimized the design of the CW Yb:YAG laser implemented during the first month for the broadband CW operation. We then inserted an etalon in order to select at least a pair of the output lasing wavelengths around 1 μm , see Fig. 7. This etalon was made from a YAG crystal. It has a diameter of 5 mm and thickness of 50 μm . It was

purchased from LightMachinery in Canada. The frequency spacing, which is the free spectral range of an etalon, is given by

$$\Delta\nu = \frac{c}{2nd \cos\theta} \quad (1)$$

where c is the speed of light in vacuum, n is the index of refraction of the etalon, d is the thickness of the etalon, and θ is the angle of the incidence. Using $n \approx 1.82$ at $1 \mu\text{m}$ [1], $d \approx 50 \mu\text{m}$, and $\theta \approx 0^\circ$, we can estimate the frequency spacing to be $\Delta\nu \approx 1.65 \text{ THz}$. The corresponding THz output wavelength generated by the difference frequency generation is $182 \mu\text{m}$. Using the setup illustrated by Fig. 7, we have measured the spectra of the laser output beam at different angles of incidence, see Fig. 8. According to Fig. 2, when the angle of incidence is $\theta \approx 6^\circ$, the spectrum consists of two peaks at the wavelengths of 1035.64 nm and 1041.72 nm , respectively. Therefore, the frequency spacing is determined to be 1.69 THz using such two wavelengths. The corresponding THz output wavelength generated by the difference frequency generation is $177 \mu\text{m}$. This experimental value deviates from the theoretical value by 2.4% . The term of $\cos\theta$ in Eq. (1) only contributes to the relative difference by 0.6% . The rest of the deviation (i.e. 1.8%) is most likely caused by the fabrication error.

Therefore, within the second month of the SBIR Phase-I contract, we have successfully demonstrated the dual-frequency operation of a CW Yb:YAG laser.

Within the third month, we have made significant progress in order to meet the Phase-I objective #1 being set in our proposal, i.e. “To demonstrate dual-frequency operation of CW and Q-switched Yb:YAG lasers”. Indeed, we have successfully achieved the Q-switched operation of the Yb:YAG laser after placing a Q-switch inside the cavity of the laser. Fig. 9 illustrates the experimental layout for our Q-switched Yb:YAG laser. A 940-nm fiber-coupled laser diode (LD) was used as a pump source. An anti-reflection-coated Yb:YAG ($C_{\text{Yb}} = 5 \text{ at. \%}$) with dimensions of 5 mm (length) and 5 mm (diameter) was used. An uncoated $50\text{-}\mu\text{m}$ -thick solid YAG etalon was inserted in the cavity to tune and select the output frequencies of the laser. The transmittance of the output coupler was $T \approx 2\%$ and the total cavity length was about 5 cm .

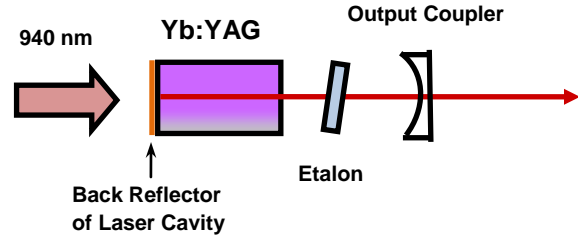


Fig. 7. A simplified experimental setup for a CW Yb:YAG laser being implemented by us during the second month. The laser cavity consists of the back reflector being directly fabricated on the Yb:YAG crystal shown in the figure and an output coupler. A YAG etalon was inserted inside the CW laser cavity for selecting a pair of the output wavelengths.

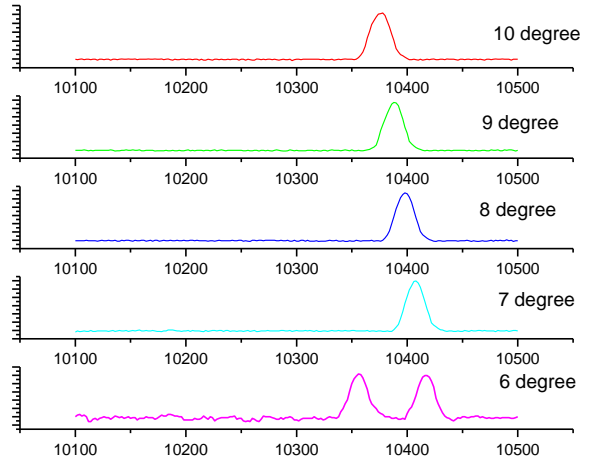


Fig. 8. Spectra of the output power generated by the operational CW Yb:YAG laser at different angles of incidence for the laser beam, i.e. θ in Eq. (1). Each vertical axis corresponds to the output power of the laser beam given in arbitrary unit whereas each horizontal axis stands for the laser output wavelength given in angstrom. A pair of the output laser wavelengths is generated at $\theta \approx 6^\circ$, see the bottom plot.

Fig. 10 shows our measurement of the output power from the Q-switched Yb:YAG laser at the repetition rate of 4 kHz as a function of the input power from the LD at 940 nm. The output power more or less linearly increases with increasing the pump power above the threshold. The slope efficiency can be determined to be 5.11% by linearly fitting the data points in Fig. 10. Such a low slope efficiency is due to the fact that a large amount of the laser power is reflected from the intra-cavity etalon. Indeed, the etalon must be rotated with its surface normal being away from the axis of the laser cavity in order to effectively select the dual frequencies. As a result, the loss of the laser cavity is significantly increased due to the reflections. There was also a reflection loss of about 25% for the pump beam at 940 nm by the surfaces of the Yb:YAG crystal. Such a loss originates from the relatively low quality of the anti-reflection coatings on the crystal. We can significantly improve the slope efficiency by resolving these issues. Furthermore, by overcoming the thermal lensing effect encountered in the experiment, we can further improve the slope efficiency. Indeed, during our experiment, we have realized that the Yb:YAG laser crystal used in our experiment suffers from the thermal lensing effect. According to Fig. 10, the threshold pump power is determined to be 3.30 W through the linear fit.

In the future, we are planning to replace the single Yb:YAG laser crystal by an adhesive-free-bond composite Yb:YAG material. Such a gain medium consists of three sections, i.e. an Yb:YAG crystal sandwiched by two undoped YAG crystals. Based on our previous result [2], such a composite material can be used to reduce the thermal lensing effect, and therefore, reduce the lasing threshold and increase the slope efficiency. We will also vary the Yb

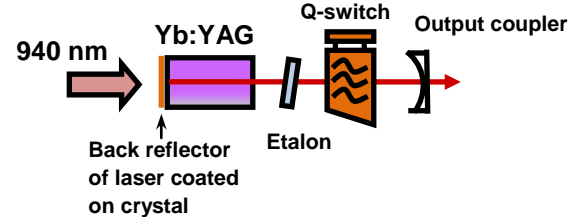


Fig. 9. A layout for a Q-switched Yb:YAG laser being implemented by us during the third month.

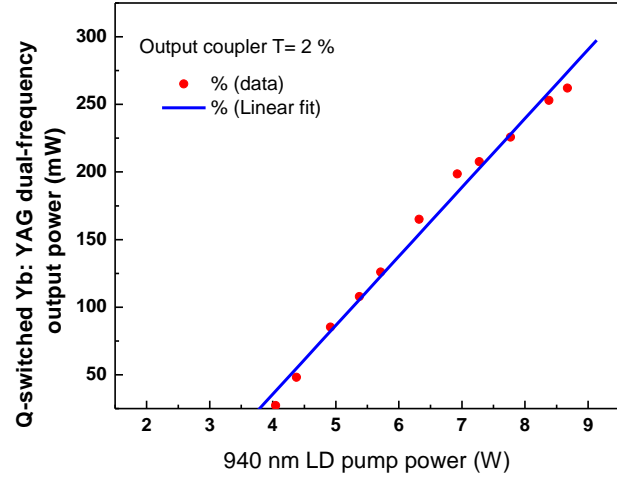


Fig. 10. Output power generated by an operational Q-switched Yb:YAG laser vs. the incident power from the LD at 940 nm.

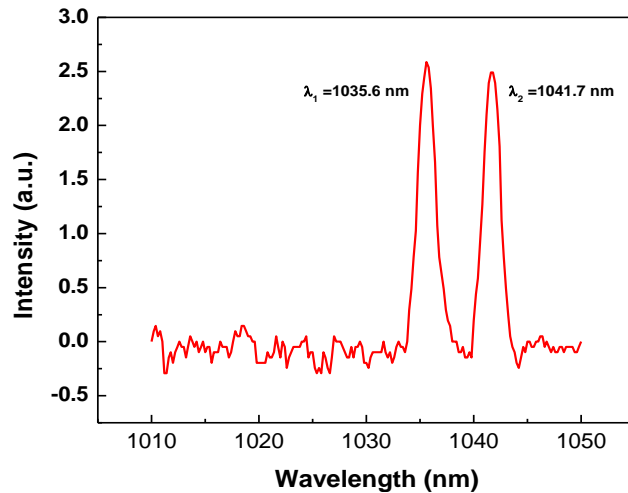


Fig. 11. Spectrum of the output generated by the Q-switched laser measured by using a spectrometer. A pair of the peaks can be seen in the spectrum, corresponding to the dual-frequency output.

doping concentration to find the optimal value.

As mentioned above, the YAG etalon is used to select a pair of the frequencies from the Q-switched Yb:YAG laser. We have measured the spectrum of the output from the laser by using a spectrometer. According to Fig. 11, a pair of the peaks at the wavelengths of 1035.6 nm and 1041.7 nm clearly appear in the spectrum, correspond to the frequencies of 289.69 THz and 287.99 THz, respectively. The difference between these two output frequencies is estimated to be 1.70 THz. This value is quite close to the theoretical value of 1.65 THz, calculated by using the refractive index of 1.82 for the YAG etalon and its thickness of 50 μm .

Therefore, within the third month of the SBIR Phase-I contract, we have successfully demonstrated the dual-frequency operation of a Q-switched Yb:YAG laser.

Within the fourth month, we have made very impressive progress in order to meet the Phase-I objective #2 being set in our proposal, i.e. “To demonstrate THz generation based on DFG outside an Yb:YAG laser cavity.”

A 940-nm fiber-coupled laser diode (LD) is used as a pump source. An anti-reflection-coated Yb:YAG ($C_{\text{Yb}} = 5$ at. %) with dimensions of 5 mm (length) and 5 mm (diameter) is used. An uncoated 50- μm -thick solid YAG etalon is inserted in the cavity to tune and select the output frequencies of the laser. The transmittance of the output coupler is $T \approx 2\%$ and the total cavity length is set to 5 cm. For our experiment on the THz generation, we set the repetition rate to 4 kHz. The pulse width of the dual-frequency output is measured to be 100 ns. A pair of the peaks at the wavelengths of 1035.6 nm and 1041.7 nm is generated. As a result, the difference between these two output frequencies from the dual-frequency Yb:YAG laser is set to 1.70 THz. The beam radius at the dual wavelengths is measured to be 150 μm near the output coupler. We have adjusted the orientation of the YAG etalon such that the output powers at the two wavelengths are nearly the same. This way, we are able to achieve the optimal THz output power based on difference-frequency generation (DFG) under the same combined pump power. We have used a plano-convex lens with the focal length of 15 cm to focus the dual-frequency beams onto the nonlinear crystal for the THz generation based on DFG.

We have used a semi-insulating (110) GaP crystal which has the thickness of 1.3 mm as the interaction length for DFG. We have measured the THz output power as a function of the total input power from the Yb:YAG laser. Fig. 12 shows our result. Based on the least squares fit illustrated by Fig. 12, the dependence based on the data points is quite close to quadratic, which is a characteristic behavior for the THz generation based on DFG. At the total input power of 250 mW (approximately 125 mW at each pump wavelength), the THz output power has reached 130 pW. *To the best of our knowledge, this is the first*

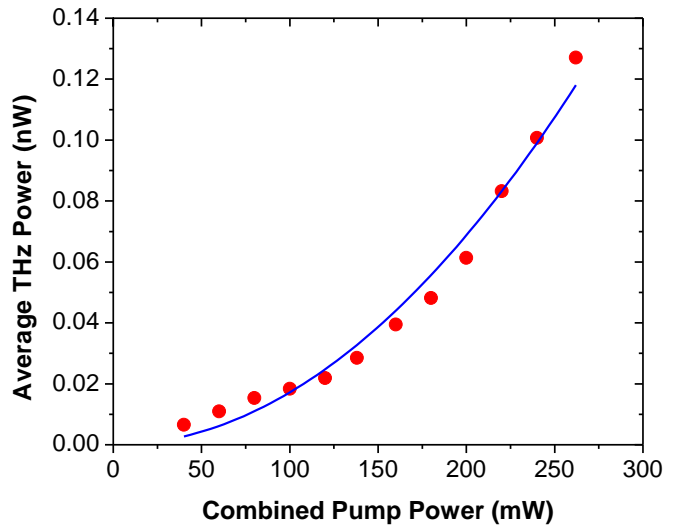


Fig. 12. Average THz power is measured as a function of the combined pump power at the dual frequencies, generated by a compact and portable Q-switched Yb:YAG laser. Solid curve represents the least squares quadratic fit to data points.

demonstration of the THz generation based on DFG from a Q-switched dual-frequency Yb:YAG laser. Our observation can be regarded as reaching an important milestone, i.e. since an Yb:YAG laser can produce a gain within a wide frequency range, DFG based on a dual-frequency Yb:YAG laser may emerge as one of the most important schemes for implementing a compact and portable THz source. Based on our estimate, the output frequencies based on such a scheme can be tuned within a wide range of 0.1 cm^{-1} - 288 cm^{-1} . Such a tuning range is perfect for identification and detection of biological agents.

We have also measured the dependence of the THz output power on the azimuth angle of the GaP crystal, see Fig. 13. One can see that the THz output power vs. the azimuth angle exhibits a nearly perfect sinusoidal oscillation, which is consistent with the theoretical prediction illustrated by the solid curve in Fig. 13.

Therefore, within the fourth month of the SBIR Phase-I contract, *we have reached one of the most important milestones*, i.e. we have successfully demonstrated the THz generation based on DFG using a compact and portable Q-switched dual-frequency Yb:YAG laser. *Such a demonstration should be regarded as a technology breakthrough.* Based on such a scheme, a compact, portable, and tunable THz source will soon become available.

Within the fifth month of the Phase-I contract, we have made very impressive progress in order to meet the Phase-I objective #3 being set in our proposal, i.e. “To carry out feasibility studies on intracavity THz generation based on the performance of the CW and Q-switched Yb:YAG lasers achieved and outer-cavity THz generation.”

In order to achieve the efficient THz generation under the intracavity configuration, it is important for us to measure the absorption of a GaP crystal in the THz region. According to Fig. 14, at the wavelength of $176 \mu\text{m}$ (the frequency of 1.70 THz), the absorption coefficient is deduced to be 0.386 cm^{-1} after removing the contribution from the Fabry-Perot effect (i.e. the modulations appearing in Fig. 14).

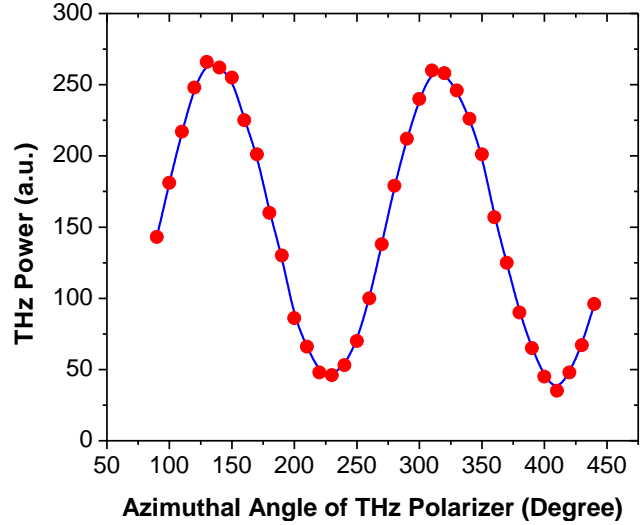


Fig. 13. THz output power is measured a function of azimuth angle of a polarizer. Solid curve stands for the nonlinear least squares fit to data points.

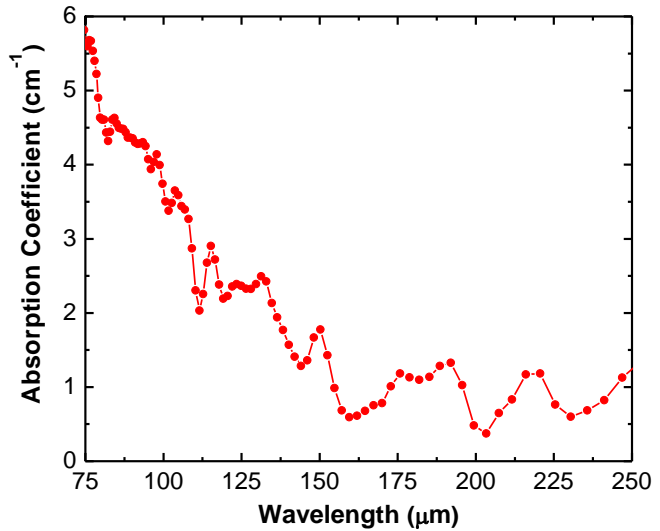


Fig. 14. Absorption coefficient is plotted vs. wavelength for a GaP crystal.

On the other hand, at the wavelengths of around 1 μm , the absorption coefficient is about 0.49 cm^{-1} [3]. When the GaP crystal is sufficiently thick, the absorption loss at such wavelengths plays the dominating role in the cavity losses for the Yb:YAG laser. Since we do not care for the power output for the Yb:YAG laser being coupled out of the output coupler, we can use two cavity mirrors with sufficiently high reflectivities (e.g. $\geq 99.9\%$) such that the reflection losses through these mirrors are negligible, compared with the absorption loss in the GaP crystal. Using the absorption loss dictated by the absorption coefficient, the maximum length of the crystal can be determined. On the other hand, for the thickness of the GaP crystal to be $663\text{ }\mu\text{m}$, the absorption loss is estimated to be 6.29% after a round trip. In such a case, the laser power at each wavelength inside the laser cavity is a factor of around 20 higher than that outside the laser cavity. As a result, the THz output power can be increased by a factor of 400. By increasing the pump power from 125 mW at each wavelength to 5 W, we will gain another factor of 1600. Therefore, the THz output power can be scaled up to $42\text{ }\mu\text{W}$. *This value is five orders of magnitude higher than the noise level of our pyroelectric detector operating at room temperature (0.23 nW).* In order to further increase the THz output power, we need to introduce a new technique. Indeed, it was recently demonstrated that when a passive Q-switch is introduced in the cavity of the Yb:YAG laser [4], the pulse width is reduced to 7 ns. Since the pulse width achieved by us so far is 100 ns, the reduction of the pulse width down to 7 ns would result in an increase in the peak power by a factor of 14.2. Since the THz peak power is proportional to the product of the peak powers at the two pump wavelengths, such a pulse-narrowing technique can provide us with an enhancement factor of 200. Therefore, at the pump power level of 5 W, the THz output power is expected to reach 8.5 mW. Such an output power corresponds to the conversion efficiency of 28%. This value approaches the record-high value of 40% set by us recently [5].

We have also considered other schemes for enhancing the THz output powers outside the laser cavity. First of all, we can utilize the total internal reflections for both the pump and THz beams inside a GaP slab. At $176\text{ }\mu\text{m}$ the absorption loss limits the interaction length to be 2.6 cm, which is amounted to an enhancement factor of about 40. Using the pulse width of 7 ns and pump power of 5 W at each wavelength, the THz output power is estimated to be $1.0\text{ }\mu\text{W}$. At longer wavelengths, the enhancement factors can be an order of magnitude larger, and therefore, the output power is increased to $10\text{ }\mu\text{W}$. On the other hand, by using metallic gratings [6], we can reduce the beam diameter from $200\text{ }\mu\text{m}$ down to $10\text{ }\mu\text{m}$. As a result, the THz output power can be increased by a factor of 400. Consequently, the THz output power can be increased to the range of 0.41 mW - 4.1 mW .

Within the sixth month of the Phase-I contract, we have made very impressive progress in order to meet the Phase-I objective #4 being set in our proposal, i.e. "To develop plan for identification and detection of biological agents."

Based on Ref. [7], *Bacillus Subtilis*, a simulant for Anthrax, exhibited unique features above 1 THz. In Ref. [8], five transition peaks from 327 GHz to 1075.5 GHz were used as absorption signatures for *Bacillus Subtilis*. Besides *Bacillus Subtilis*, Soman and Sarin, i.e. warfare agents, exhibited a series of rotational transitions [7]. THz spectroscopy was assessed as an effective technique for remote detection of biological warfare agents [9]. For toxin Ovalbumin, bacteria *Erwinia herbicola*, *Bacillus Subtilis*, lyophilized cells, RNA MS2 phage, and BioGene, signatures were found within $3\text{-}10\text{ cm}^{-1}$ [10]. Transmission spectra of Ovalbumin were also measured in $15\text{-}680\text{ cm}^{-1}$ [11], see Fig. 15.

According to Fig. 15, we could only identify four transition peaks. We believe this is due to the large background originating from the scattering of the THz waves by the Ovalbumin sample. The non-oscillatory decreases of the transmittances as the frequency is increased (as the wavelength is decreased) could be the manifestation of the Rayleigh scattering of the THz waves, when the grain sizes in the biological sample are much smaller the THz wavelength. Indeed, as the THz wavelength approaches the size of the Ovalbumin particles, the scattering of the THz waves can be greatly enhanced, which can be described by the resonant Mie scattering.

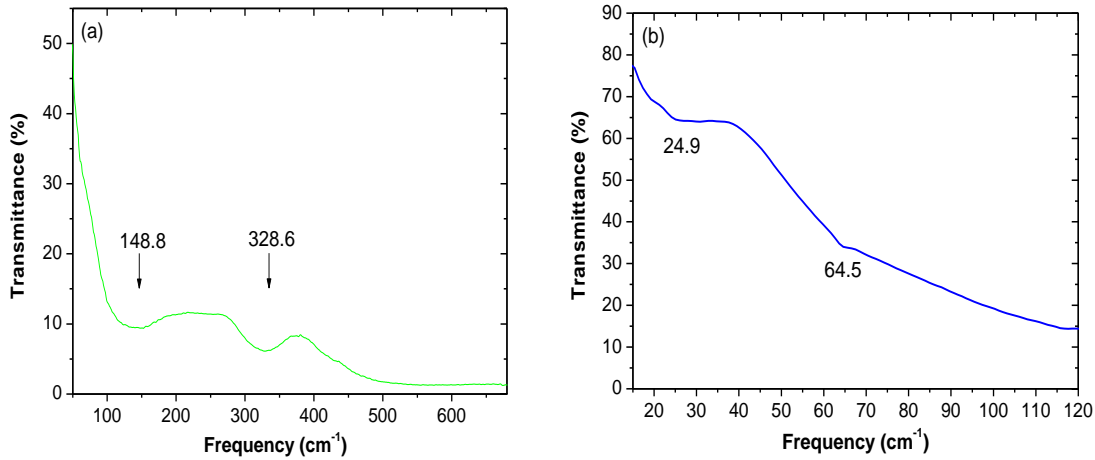


Fig. 15. Transmission spectra of Ovalbumin in the range of (a) 50-680 cm^{-1} and (b) 15-120 cm^{-1} .

From the discussion above, it would be very important for us to develop a novel scheme of removing the non-oscillatory background due to the scattering of the THz waves by the particles present in the biological samples. One possibility for subtracting such a background from the measured transmittances is to use a heterodyne detection scheme. Indeed, let us assume that we can send a pair of approximately same THz frequencies through a biological sample. If the signals at the two frequencies are phase-coherent with respect to each other, we can then remove the background by monitoring the heterodyne signal from the two transmitted signals at the slightly different frequencies. We believe that once the background is removed, we will be able to identify small absorption features which can be buried under the huge background. Obviously, there is a trade-off between the sample thickness and signal-to-noise ratio. If the sample is too thick, the multiple scattering events can become a huge background. On the other hand, if the sample is too thin, one cannot reliably measure the transmittances. Such a trade-off must be investigated in the future. One should also study the dependence of the transmittances on the particle sizes in the typical biological sample. On the other hand, there is an interference of the THz waves being reflected by the front and back surfaces of the sample. Such an interference effect will add oscillations to the spectrum of the transmittance. It can be partially removed by making measurements on a wedged sample.

For *E. coli*, transition peaks were identified in 10-25 cm^{-1} [12,13]. Based on measurements made on three bio-simulants [14], transition signatures existed in 120-750 GHz (4-25 cm^{-1}). It was demonstrated that *Bacillus Subtilis* and spores in polyethylene and dilute water solutions still exhibited resonance peaks in the THz region [15,16]. Most of these transition features origin from phonon modes [17]. THz spectroscopy of DNA was carefully investigated in 10-25 cm^{-1} [17-19], see Fig. 16. In addition to DNA, proteins [20], insulins [21], and glucose [22] were

fingerprinted. THz spectroscopic technique was also used to characterize cancer cells in $10\text{-}25\text{ cm}^{-1}$ [23]. It is important for us to point out that in most of the reports summarized above the spectroscopic studies have been carried out by using Fourier transform infrared spectroscopy (FTIR). Such an instrument is rather bulky. In addition, it cannot be used to achieve remote detections. Moreover, the radiation source used in FTIR for covering the range of $3\text{-}25\text{ cm}^{-1}$ produces low output powers. Therefore, THz spectroscopy based on FTIR suffers from greatly reduced sensitivities. Furthermore, relatively high spectral resolutions cannot be achieved by a compact FTIR spectrometer.

During Phase II, we plan to combine our THz emitter with a pyroelectric detector operating at room temperature to construct a compact and portable spectrometer. This spectrometer will meet the requirement of the average output power of 1 mW, peak power of 20 W, a continuously frequency-tuning range of $150\text{ GHz} - 1\text{ THz}$ ($5\text{-}33.3\text{ cm}^{-1}$), a linewidth of 100 MHz, a repetition rate of 10 kHz, and a system dimension footprint of $10''\times 6''\times 4''$ or smaller. Our goal is to implement a prototype spectrometer by the end of Phase II. We expect that shortly after the end of Phase II, ArkLight will be ready for taking orders of the spectrometers. It is worth noting that for the input power of 1 mW, the dynamic range for measuring attenuation of the THz wave can be as high as 4×10^6 by using a sensitive pyroelectric detector working at room temperature. This implied that for the sample thickness of 1 mm, the absorption coefficient can be as high as 150 cm^{-1} . On the other hand, for the absorption coefficient of 1 cm^{-1} , the measurable penetration depth is 15 cm.

We will choose toxin Ovalbumin, *Bacillus Subtilis*, RNA from MS2 phage, and *E. coli* to test our spectrometer in the range of $5\text{-}33.3\text{ cm}^{-1}$. We will compare our measurements of the spectra with those made by using FTIR [7-14]. Our goal is to demonstrate the advantages of our novel spectrometer in terms of sensitivity, spectral resolution, linewidth, tuning range, scanning speed, capability of sensing in the reflection mode, dynamic range, and false alarm rate due to artifact. We will investigate the feasibility of removing the background due to the Rayleigh scattering of the THz wave by the grain particles present in the biological samples, as discussed above.

References

- [1] W. Koechner and M. Bass, *Solid-State Lasers*, Springer, NY, 2003.
- [2] P. Zhao, Y. J. Ding, and I. B. Zotova, "Power scaling of blue and red light based on frequency mixing inside adhesive-free bond composite Nd:YAG laser cavity," *Opt. Commun.* 283, 1905-1908 (2010).
- [3] D. N. Nikogosyan, *Properties of optical and laser-related materials*, Wiley, NY, 1997.

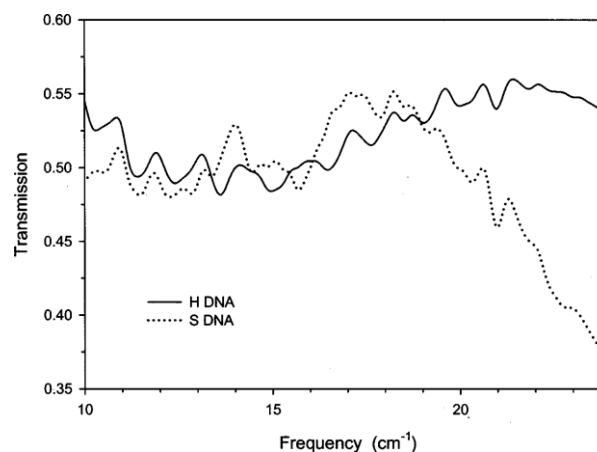


Fig. 16. A comparison of salmon and herring DNA transmission spectra taken from Ref. [17].

- [4] M. Yakshin, C. R. Prasad, G. Schwemmer, M. Banta, and I. H. Hwang, "Compact, diode-pumped Yb:YAG laser with combination acoustic-optic and passive Q-switch for LIDAR applications," JWA46, CLEO 2011.
- [5] Y. Jiang, D. Li, Y. J. Ding, and I. B. Zotova, "Terahertz Generation Based on Parametric Conversion: From Saturation of Conversion Efficiency to Back Conversion," Opt. Lett. **36**, 1608-1610 (2011).
- [6] Q. Gan, Z. Fu, Y. J. Ding, and F. J. Bartoli, "Ultra-wideband slow light system based on THz plasmonic graded metallic grating structures," Phys. Rev. Lett. **100**, 256803/1-4, (2008).
- [7] D. Woolard, R. Kaul, R. Suenram, A. H. Walker, T. Globus, and A. Samuels, "Terahertz electronics for chemical and biological warfare agent detection," 1999 IEEE MTT-S Digest, pp. 925-928.
- [8] E. R. Brown, D. L. Woolard, A. C. Samuels, T. Globus, and B. Gelmont, "Remote detection of bioparticles in the THz region," 2002 MTT-S Digest, pp. 1591-1594.
- [9] D. L. Woolard, E. R. Brown, A. C. Samuels, J. O. Jensen, T. Globus, B. Gelmont, and M. Wolski, "Terahertz-frequency remote-sensing of biological warfare agents," 2003 MTT-S Dig., pp. 763-766.
- [10] T. Globus, D. Woolard, T. Khromova, R. Partasarathy, A. Majewski, R. Abreu, J. L. Hesler, S.-K. Pan, and G. Ediss, "Terahertz signatures of biological-warfare-agent simulants," SPIE **5411**, 25-32 (2004).
- [11] R. Song, Y. J. Ding, and I. B. Zotova, "Fingerprinting Ovalbumin – simulant of protein toxins in extremely-wide frequency range," JWA57, CLEO 2010, May 16-21, San Jose, CA.
- [12] A. Bykhovski, X. Li, T. Globus, T. Khromova, B. Gelmont, D. Woolard, A. C. Samuels, and J. O. Jensen, "THz absorption signature detection of genetic material of *E. coli* and *B. subtilis*," SPIE **5995**, 59950N/1-10 (2005).
- [13] A. Bykhovski, T. Globus, T. Khromova, B. Gelmont, and D. Woolard, "Resonant terahertz spectroscopy of bacterial thioredoxin in water: simulation and experiment," Intern. J. High Speed Electron. Sys. **18**, 109-117 (2008).
- [14] A. Majewski, P. Miller, R. Abreu, J. Grotts, T. Globus, and E. Brown, "Terahertz signature characterization of bio-simulants," SPIE **5790**, 74-84 (2005).
- [15] T. Globus, T. Khromova, D. Woolard, and A. Samuels, "THz resonance spectra of bacillus subtilis cells and spores in PE pellets and dilute water solutions," SPIE **6212**, 62120K/1-12 (2006).
- [16] A. Bykhovski, T. Globus, T. Khromova, B. Gelmont, and D. Woolard, "An analysis of the THz frequency signatures in the cellular components of biological agents," Intern. J. High Speed Electron. Sys. **17**, 225-237 (2007).
- [17] D. L. Woolard, T. R. Globus, B. L. Gelmont, M. Bykhovskaia, A. C. Samuels, D. Cookmeyer, J. L. Hesler, T. W. Crowe, J. O. Jensen, J. L. Jensen, and W. R. Loerop, "Submillimeter-wave phonon modes in DNA macromolecules," Phys. Rev. E **65**, 051903/1-11 (2002).
- [18] T. R. Globus, D. L. Woolard, A. C. Samuels, B. L. Gelmont, J. Hesler, T. W. Crowe, and M. Bykhovskaia, "Submillimeter-wave Fourier transform spectroscopy of biological macromolecules," J. Appl. Phys. **91**, 6105-6113 (2002).

- [19] T. Globus, D. Woolard, T. W. Crowe, T. Khromova, B. Gelmont, and J. Hesler, "Terahertz Fourier transform characterization of biological materials in a liquid phase," *J. Phys. D: Appl. Phys.* **39**, 3405-3413 (2006).
- [20] W. Shi and Y. J. Ding, "A monochromatic and high-power THz source tunable in the ranges of 2.7-38.4 μm and 58.2-3540 μm for variety of potential applications," *Appl. Phys. Lett.* **84**, 1635-1637 (2004).
- [21] R. Song, Y. J. Ding, and Y. B. Zotova, "Fingerprinting insulins in the spectral region from mid-IR to THz," *Intern. J. High Speed Electron. Sys.* **17**, 251-260 (2007).
- [22] R. Song, Y. J. Ding, and I. B. Zotova, "Newly identified transition peaks of Glucose in wide frequency range using new spectroscopic technique," submitted to *Appl. Opt.*
- [23] T. Globus, D. Theodorescu, H. Frierson, T. Khromova, and D. Woolard, "Terahertz spectroscopic characterization of cancer cells," *SPIE* **5692**, 233-240 (2005).